Comput Visual Sci (2005) 8(2): 49–68
DOI 10.1007/s00791-005-0152-9

Computing and
Visualization in Science

REGULAR ARTICLE

T. Bubeck · R. Hiptmair · H. Yserentant

The finite mass mesh method

Received: 11 March 2003 / Accepted: 24 November 2004 / Published online: 23 September 2005

Communicated by: G. Wittum

Abstract The finite mass method is a purely Lagrangian scheme for the spatial discretisation of the macroscopic phenomenological laws that govern the flow of compressible fluids. In this article we investigate how to take into account long range gravitational forces in the framework of the finite mass method. This is achieved by incorporating an extra discrete potential energy of the gravitational field into the Lagrangian that underlies the finite mass method. The discretisation of the potential is done in an Eulerian fashion and employs an adaptive tensor product mesh fixed in space, hence the name *finite mass mesh method* for the new scheme. The transfer of information between the mass packets of the finite mass method and the discrete potential equation relies on numerical quadrature, for which different strategies will be proposed. The performance of the extended finite mass method for the simulation of two-dimensional gas pillars under self-gravity will be reported.

1 Introduction

The finite mass method gives a discrete macroscopic description of the flow of a compressible fluid. It is a purely Lagrangian approach based on first principles of fluid mechanics. The main idea is to discretise the fluid by means of a finite number of mass packets which are called "particles". These particles have finite extension, move independently, and can intersect and penetrate each other. Their motion is determined by internal and external forces, and they obey the laws of thermodynamics. The finite mass method was introduced by C. Gauger, P. Leinen, and H. Yserentant in [9] and is an extension of earlier works of Yserentant: whereas in [21] the particles have a fixed shape and size, they are allowed to change their size in [23]. Finally, in [9] the model is supplemented such that the particles can even change their shape by linear deformations. Extensions and special variants are described in [14, 15].

The main merit of the finite mass method is its fairly comprehensive rigorous theoretical underpinning. In [21, 22] compactness and convergence results for simpler variants of the finite mass method are given, and in the case of flows with given force and velocity fields its convergence is analysed in [25]. The propagation of sound is studied in [24] for a simplified particle model.

The finite mass method is a new member of a large class of Lagrangian schemes in computational fluid dynamics. Another representative are techniques known as smoothed particle hydrodynamics [1, 20], which are widely used in computational astrophysics. Many strategies have been devised to model long range graviational interactions in these schemes, some based on so-called tree methods [12] some on the discretisation of elliptic PDEs on Eulerian grids [7].

The latter idea will be pursued in this paper: we will rely on a finite element discretisation of the potential equation on a mesh fixed in space. This mesh will undergo dynamic adaptation to reflect the distribution of mass. Crucial will be the transfer of information between the particles and the discrete variational problem on the Eulerian mesh. Besides theoretical investigations of the fully coupled (semidiscrete) scheme, this new aspect of information transfer will receive much attention in this paper.

A brief outline of the paper is as follows: In the next section we present a short introduction to the finite mass method, closely following [9]. In the third section we extend the semi-discrete finite mass method to cover effects due to the potential field created by the mass of the particles. Since these effects result in force terms containing integrals

T. Bubeck
SFB 382, Universität Tübingen, D-72076 Tübingen, Germany
E-mail: tanja_bubeck@web.de

R. Hiptmair (✉)
Seminar for Applied Mathematics, ETH Zürich, CH-8092 Zürich, Switzerland
E-mail: hiptmair@sam.math.ethz.ch

H. Yserentant
Institut für Mathematik, TU Berlin, D-10623 Berlin, Germany
E-mail: yserentant@math.tu-berlin.de

which cannot be evaluated exactly, their discretisation is described in Sect. 4. The fifth section deals with some aspects of the implementation. In addition to the implementation of the force terms, adaptive mesh refinement, and the total computational costs are discussed. Finally, in Sect. 6, we report some illustrative computational experiments of gas columns under the influence of self-gravitation.

2 The finite mass method

2.1 The description of a particle

The mass packets that describe the distribution of the fluid matter in the finite mass method are characterised by an internal mass distribution that is given by a fixed continuously differentiable shape function $\psi : \mathbb{R}^d \to \mathbb{R}^+$, $d \in \mathbb{N}$, on a reference particle. This shape function has compact support, is nonnegative, and satisfies

$$\int_{\mathbb{R}^d} \psi(y)\, dy = 1, \quad \int_{\mathbb{R}^d} \psi(y) y\, dy = 0, \tag{1}$$

which means that the total reference mass is 1, and that the barycentre of the reference particle is the origin. Further, the reference particle has identical principal moments of inertia

$$\int_{\mathbb{R}^d} \psi(y) y_k y_l\, dy = J \delta_{kl}, \tag{2}$$

where y_k are the components of $y \in \mathbb{R}^d$ and $J \in \mathbb{R}^+$. In the computational examples of Sect. 6, for the shape function ψ we use the tensor product of normalised third order B-splines as in [8, 9].

Then, arbitrary particles are obtained by linear affine transformations of the reference particle. The motion of a particle labelled with index i is described by the trajectories $x_y(\cdot) \in \mathbb{R}^d$ of the points y belonging to the reference particle as follows:

$$x_y : \mathbb{R}^+ \to \mathbb{R}^d : t \mapsto q_i(t) + H_i(t) y,$$

where $q_i(t) \in \mathbb{R}^d$ determines the position of the barycentre of the particle and $H_i(t) \in \mathbb{R}^{d\times d}$ with $\det H_i(t) > 0$ its deformation at time t. This deformation matrix H_i determines the orientation in space, the shape, and the size of the particle.

The velocity of the points of a particle is seen to be

$$t \to q_i'(t) + H_i'(t) y,$$

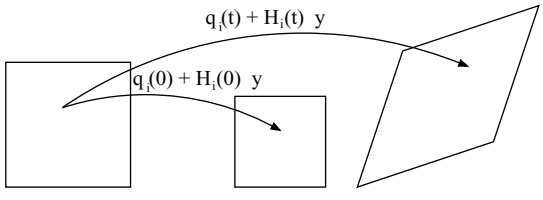

Fig. 1 Motion of a particle with index (label) i

by which we obtain the velocity field of a particle with respect to space coordinates as

$$v_i(x,t) = q_i'(t) + H_i'(t) H_i(t)^{-1} (x - q_i(t)).$$

Accordingly, the normed transformed shape function $\psi_i(x,t)$ of the reference particle corresponding to the ith particle is given by (cf. [9, Eq. (2.17)])

$$\psi_i(x,t) := \frac{\psi(H_i^{-1}(t)(x - q_i(t)))}{\det(H_i(t))}.$$

With $m_i \in \mathbb{R}^+$ denoting the mass of the particle, we obtain its mass density by $m_i \psi_i(x,t)$.

2.2 Global quantities

From quantities of the individual particles, global quantities like the total mass density and the velocity field can be derived. For the sake of lucidity, in the following we occasionally omit the dependence on time in the notation (in particular for q_i and H_i).

The total mass density is given by superposition of the mass densities of the individual particles

$$\rho(x,t) := \sum_{i=1}^{N} m_i \psi_i(x,t), \tag{3}$$

where $N \in \mathbb{N}$ denotes the number of particles.

Since the particles can intersect each other and have different velocities, the total velocity field at a point in space is not given directly. To obtain the velocity field of the flow, we first look at the total mass flux density, which is given by superposition of the mass flux densities of the individual particles

$$j(x,t) := \sum_{i=1}^{N} m_i \psi_i(x,t) v_i(x,t).$$

Since the velocity field v of the flow is defined by the relation $j(x,t) = \rho(x,t) v(x,t)$, it has the form

$$v(x,t) = \sum_{i=1}^{N} \chi_i(x,t) v_i(x,t), \tag{4}$$

with the local mass fraction

$$\chi_i(x,t) := \frac{m_i \psi_i(x,t)}{\rho(x,t)}. \tag{5}$$

In order to describe the thermodynamic state of a fluid, a second thermodynamic quantity besides the mass density is required. The finite mass method uses the entropy density s which is given by

$$s(x,t) := \sum_{i=1}^{N} m_i S_i(t) \psi_i(x,t),$$

where $S_i(t) \in \mathbb{R}$ denotes the specific entropy of the ith particle at time t. If the specific entropies are constant in time, the particles are thermically isolated from each other.

By Gibbs fundamental relation, the pressure π and the temperature θ can be expressed through the internal energy ε per unit volume, the mass density ρ, and the entropy density s according to[1]

$$\pi(\rho,s)=\frac{\partial\varepsilon}{\partial\rho}\rho+\frac{\partial\varepsilon}{\partial s}s-\varepsilon,\quad \theta(\rho,s)=\frac{\partial\varepsilon}{\partial s}.$$

More details can be found in [21].

2.3 Equations of motion

To derive the equations of motion of the particles by the Lagrangian approach, the energy of the system of particles has to be considered. In our case we can distinguish the kinetic and the internal energy.

The particle i has the kinetic energy (cf. [9, Eq. (2.31)])

$$\begin{aligned}E_i^{\mathrm{kin}}(t)&=\frac{1}{2}\int_{\mathrm{supp}(\psi_i)} m_i\psi_i(x,t)|v_i(x,t)|^2\,dx\\&=\frac{1}{2}(m_i|q_i'|^2+Jm_i|H_i'|^2),\end{aligned}$$

where $|\cdot|$ denotes the Euclidian vector norm and the Frobenius norm of a matrix, respectively. Then, the total kinetic energy is obtained by superposition of the kinetic energy of the individual particles

$$E^{\mathrm{kin}}(t):=\sum_{i=1}^{N}E_i^{\mathrm{kin}}(t).$$

The internal energy of the system is given by

$$E^{\mathrm{int}}(t)=\int_{\mathbb{R}^d}\varepsilon(\rho(x,t),s(x,t))\,dx. \tag{6}$$

The Lagrangian of the system of particles is defined by

$$\mathcal{L}(t):=E^{\mathrm{kin}}(t)-E^{\mathrm{int}}(t),$$

which determines the motion of the particles by the Lagrange equations (cf. [9, Eq. (2.36)])

$$\frac{d}{dt}\frac{\partial\mathcal{L}}{\partial q_i'}-\frac{\partial\mathcal{L}}{\partial q_i}=0,\quad \frac{d}{dt}\frac{\partial\mathcal{L}}{\partial H_i'}-\frac{\partial\mathcal{L}}{\partial H_i}=0. \tag{7}$$

Note that the kinetic energy E^{kin} does not depend on q_i and H_i whereas the internal energy E^{int} does not depend on q_i' and H_i'. Inserting the mass packets, the equations of motion for an individual particle have the form

$$\begin{aligned}m_iq_i''&=-\frac{\partial E^{\mathrm{int}}}{\partial q_i}=-\frac{\partial}{\partial q_i}\int_{\mathbb{R}^d}\varepsilon(\rho,s)\,dx,\\Jm_iH_i''&=-\frac{\partial E^{\mathrm{int}}}{\partial H_i}=-\frac{\partial}{\partial H_i}\int_{\mathbb{R}^d}\varepsilon(\rho,s)\,dx.\end{aligned}$$

[1] For the fundamentals of mechanics and fluid dynamics we refer to [11, 17] and [3, 4, 18], respectively.

The terms on the right hand side represent the forces of internal pressure. With the normalised forces

$$\begin{aligned}F_i&:=-\frac{1}{m_i}\frac{\partial E^{\mathrm{int}}}{\partial q_i}=-\int_{\mathbb{R}^d}\left\{\frac{\partial\varepsilon}{\partial\rho}+S_i\frac{\partial\varepsilon}{\partial s}\right\}\frac{\partial\psi_i}{\partial q_i}\,dx,\\M_i&:=-\frac{1}{m_i}\frac{\partial E^{\mathrm{int}}}{\partial H_i}=-\int_{\mathbb{R}^d}\left\{\frac{\partial\varepsilon}{\partial\rho}+S_i\frac{\partial\varepsilon}{\partial s}\right\}\frac{\partial\psi_i}{\partial H_i}\,dx,\end{aligned} \tag{8}$$

where the particle mass cancels, the equations of motion become

$$q_i''=F_i,\quad JH_i''=M_i. \tag{9}$$

The forces (8) can be simplified using (see [9, Sect. 2])

$$\frac{\partial\psi_i}{\partial q_i}=-\nabla\psi_i, \tag{10}$$

$$\frac{\partial\psi_i}{\partial H_i}=-[\nabla\psi_i]\big[H_i^{-1}(x-q_i)\big]^T-\psi_iH_i^{-T}. \tag{11}$$

Real fluid flow is accompanied by heat generation at shocks and due to viscosity. As described in [22, Sect. 4] and [9, Sect. 2] these effects can be taked into account in the finite mass method, too. Then, the equations of motion (9), extended by frictional (fr) and viscous (v) forces, have the form

$$q_i''=F_i+F_i^{\mathrm{fr}}+F_i^{\mathrm{v}},\quad JH_i''=M_i+M_i^{\mathrm{fr}}+M_i^{\mathrm{v}}. \tag{12}$$

2.4 Conservation properties

By virtue of the Lagrangian approach the total energy, the total momentum, and the total angular momentum are constants of motion. The total energy of the system $E^{\mathrm{tot}}:=E^{\mathrm{kin}}+E^{\mathrm{int}}$ is composed of the kinetic and the internal energy. The total momentum is defined as

$$P(t):=\int_{\mathbb{R}^d}\rho(x,t)v(x,t)\,dx=\sum_{i=1}^{N}m_iq_i'. \tag{13}$$

In three dimensions the angular momentum is given by

$$L(t):=\int_{\mathbb{R}^d}\rho(x,t)\,x\times v(x,t)\,dx. \tag{14}$$

Its components can be represented by

$$L_j(t):=\int_{\mathbb{R}^d}\rho(x,t)\,x\cdot W_j\,v(x,t)\,dx,\quad j=1,2,3, \tag{15}$$

where the product $x\cdot y:=x^Ty$, and W_j, $j=1,2,3$, are fixed skew symmetric matrices depending on the cross product. One can show that these matrices W_j build a basis of the space of skew symmetric matrices. Hence, for the conservation of the angular momentum it is sufficient to show $\frac{d}{dt}L_W(t)=0$ for an arbitrary skew symmetric matrix W with

$$L_W(t):=\int_{\mathbb{R}^d}\rho(x,t)\,x\cdot Wv(x,t)\,dx. \tag{16}$$

Theorem 1 *The total energy E^{tot}, the total momentum P, and the angular momentum L are constants of motion, i.e.*

$$\frac{d}{dt}E^{\mathrm{tot}}(t)=0,\quad \frac{d}{dt}P(t)=0,\quad \frac{d}{dt}L(t)=0.$$

For the proof we refer to [9, Sect. 3].

3 Gravitational fields

Gravitational forces are conservative forces, i.e. they can be represented by means of the gradient of a potential. In three dimensions the gravitational potential ϕ is determined by the Poisson equation,

$$\Delta\phi(x,t) = \rho(x,t), \quad x \in \mathbb{R}^3, \quad t \geq 0, \tag{17}$$

which has to be supplemented by suitable decay conditions depending on the spatial dimension d [19, Ch. 8], e.g., $\lim_{|x|\to\infty} \phi(x,t) = 0$ for $d = 3$. We remark that for simplicity the gravitational constant is set to 1. Then, the potential can be represented as the Newton potential ϕ (s. [5, Chap. 2, Sects. 2 and 3, in particular Proposition 3]) given by with the fundamental solution $\Gamma(x) = g(|x|)$. Remember that for $d = 3$ we have $\Gamma(x) = -\frac{1}{4\pi}\frac{1}{|x|}$. We point out that here and below the integration kernels $\Gamma(x-y)$ are weakly singular and all integral exists in the Lebesgue sense over $\mathbb{R}^d$. Thus, swapping integration and differentiation can always be justified.

$$\phi(x,t) = \int_{\mathbb{R}^3} \Gamma(x-y)\rho(y,t)\,dy, \quad x \in \mathbb{R}^3, \quad t \geq 0 \tag{18}$$

In the following we want to extend the Lagrangian approach of Sect. 2.3 by gravitation. Thus, we have to consider the additional energy given by the gravitational field. The potential energy is defined by

$$\begin{aligned} E^{\text{pot}}(t) &:= \frac{1}{2}\int_{\mathbb{R}^d} \phi(x,t)\rho(x,t)\,dx \\ &= \frac{1}{2}\int_{\mathbb{R}^d} |\nabla\phi(x,t)|^2\,dx, \end{aligned}$$

and using (18) and (3), it has the representation

$$\begin{aligned} E^{\text{pot}}(t) = \frac{1}{2}\sum_{i,j=1}^{N} m_i m_j \\ \times \int_{\mathbb{R}^d}\int_{\mathbb{R}^d} \Gamma(x-y)\psi_j(y,t)\psi_i(x,t)\,dy\,dx. \end{aligned}$$

It enters the Lagrangian as another additive contribution: $\mathcal{L} := E^{\text{kin}} - E^{\text{int}} - E^{\text{pot}}$.

Then, the Lagrange Eq. (7) read

$$\begin{aligned} \frac{d}{dt}\frac{\partial E^{\text{kin}}}{\partial q_i'} &= -\frac{\partial E^{\text{int}}}{\partial q_i} - \frac{\partial E^{\text{pot}}}{\partial q_i}, \\ \frac{d}{dt}\frac{\partial E^{\text{kin}}}{\partial H_i'} &= -\frac{\partial E^{\text{int}}}{\partial H_i} - \frac{\partial E^{\text{pot}}}{\partial H_i}. \end{aligned}$$

Note that the potential energy only depends on q_i and H_i. Then, the normalised forces acting on the particle i are given by the derivatives of the potential energy

$$\begin{aligned} F_i^{\text{gr}} := -\frac{1}{m_i}\frac{\partial E^{\text{pot}}}{\partial q_i} = \frac{-1}{2m_i}\frac{\partial}{\partial q_i}\sum_{k,j=1}^{N} m_k m_j \\ \times \int_{\mathbb{R}^d}\int_{\mathbb{R}^d} \Gamma(x-y)\psi_j(y,t)\psi_k(x,t)dydx. \end{aligned}$$

Since Γ is symmetric and ψ_j only depends on q_i for $j = i$, the gravitational force is given by

$$F_i^{\text{gr}} = -\int_{\mathbb{R}^d} \phi(x,t)\frac{\partial\psi_i}{\partial q_i}(x,t)\,dx. \tag{19}$$

Analogously, we obtain for the deformation matrices

$$M_i^{\text{gr}} := -\frac{1}{m_i}\frac{\partial E^{\text{pot}}}{\partial H_i} = -\int_{\mathbb{R}^d} \phi(x,t)\frac{\partial\psi_i}{\partial H_i}(x,t)\,dx. \tag{20}$$

By these considerations the equations of motion for a particle can be extended to

$$\begin{aligned} q_i'' &= F_i + F_i^{\text{fr}} + F_i^{\text{v}} + F_i^{\text{gr}}, \\ J H_i'' &= M_i + M_i^{\text{fr}} + M_i^{\text{v}} + M_i^{\text{gr}}. \end{aligned} \tag{21}$$

In Sect. 2.4 we have seen that the finite mass method conserves the total energy, the total momentum, and the total angular momentum. Now, we show that in the case of additional gravitational forces these quantities also remain constants of motion.

Theorem 2 *The total energy*

$$E^{\text{tot}}(t) := E^{\text{kin}}(t) + E^{\text{int}}(t) + E^{\text{pot}}(t) \tag{22}$$

the total momentum (13), and the total angular momentum (14) are constants of motion.

Proof To begin with, the conservation of the total energy is an immediate consequence of the Lagrangian approach.

Second, inserting the equations of motion (21) into $\frac{d}{dt}P(t)$ we obtain

$$\begin{aligned} \frac{d}{dt}P(t) &= \sum_{i=1}^{N} m_i F_i + \sum_{i=1}^{N} m_i F_i^{\text{fr}} + \sum_{i=1}^{N} m_i F_i^{\text{v}} + \sum_{i=1}^{N} m_i F_i^{\text{gr}} \\ &=: P_1' + P_2' + P_3' + P_4'. \end{aligned}$$

In [9, Sect. 3, Theorem 2] it is proved that P_1', P_2', and P_3' vanish. Thus, it remains to show that also $P_4' = 0$. Using (10), we have

$$\begin{aligned} P_4' &= -\sum_{i=1}^{N} m_i \int_{\mathbb{R}^d} \phi(x)\frac{\partial\psi_i}{\partial q_i}(x)\,dx \\ &= \sum_{i=1}^{N} m_i \int_{\mathbb{R}^d} \phi(x)\nabla\psi_i(x)\,dx = \int_{\mathbb{R}^d} \phi(x)\nabla\rho(x)\,dx. \end{aligned}$$

Now, we insert the potential given in (18). Since ρ has compact support, integration by parts yields

$$\begin{aligned} &\int_{\mathbb{R}^d} \phi(x)\nabla_x\rho(x)\,dx \\ &\quad= \int_{\mathbb{R}^d}\int_{\mathbb{R}^d} \Gamma(x-y)\rho(y)\,dy\,\nabla_x\rho(x)\,dx \\ &\quad= -\int_{\mathbb{R}^d}\int_{\mathbb{R}^d} \nabla_x\Gamma(x-y)\rho(y)\,dy\,\rho(x)\,dx. \end{aligned}$$

Using $\nabla_x \Gamma(x-y) = -\nabla_y \Gamma(x-y)$, we find that $P_4' = 0$:

$$\int_{\mathbb{R}^d} \phi(x) \nabla_x \rho(x)\, dx = -\int_{\mathbb{R}^d} \phi(y) \nabla_y \rho(y)\, dy.$$

Finally, we prove the conservation of the total angular momentum. We have to show that the time derivative of the quantity defined in (16) vanishes for arbitrary skew symmetric matrices W. With (1), (2), and (4), we obtain

$$\begin{aligned}\frac{d}{dt} L_W(t) &= \frac{d}{dt} \int_{\mathbb{R}^d} \rho(x,t) x \cdot W v(x,t)\, dx \\ &= \sum_{i=1}^N \frac{d}{dt} \big(m_i q_i \cdot W q_i' + J m_i H_i \cdot W H_i' \big) \\ &= \sum_{i=1}^N \big(m_i q_i \cdot W q_i'' + J m_i H_i \cdot W H_i'' \big).\end{aligned}$$

For the last equality we have used that $a \cdot Wa = 0$ for all vectors $a \in \mathbb{R}^d$ and $A \cdot WA = 0$ for all square matrices $A \in \mathbb{R}^{d\times d}$.[2] Now, inserting the equations of motion (21) yields

$$\begin{aligned}\frac{d}{dt} L_W(t) \;=\; & \sum_{i=1}^N m_i (q_i \cdot W F_i + H_i \cdot W M_i) \\ & + \sum_{i=1}^N m_i \big(q_i \cdot W F_i^{\mathrm{fr}} + H_i \cdot W M_i^{\mathrm{fr}} \big) \\ & + \sum_{i=1}^N m_i \big(q_i \cdot W F_i^{\mathrm{v}} + H_i \cdot W M_i^{\mathrm{v}} \big) \\ & + \sum_{i=1}^N m_i \big(q_i \cdot W F_i^{\mathrm{gr}} + H_i \cdot W M_i^{\mathrm{gr}} \big) \\ =:\; & L_1' + L_2' + L_3' + L_4'.\end{aligned}$$

It is shown in [9, Sect. 3, Theorem 3] that the first three terms vanish separately. Hence, we only have to consider L_4'. For the following computations, we recall (10) and (11). Moreover, we use that

$$A \cdot Bab^T = Ab \cdot Ba, \quad A \cdot (BC) = (AC^T) \cdot B \tag{23}$$

holds for all square matrices A, B, and C, and all vectors a and b. With these relations we obtain

$$q_i \cdot W \frac{\partial \psi_i}{\partial q_i} + H_i \cdot W \frac{\partial \psi_i}{\partial H_i} = Wx \cdot \nabla \psi_i.$$

Now, inserting the gravitational forces (19) and (20) in L_4' yields

$$\begin{aligned}L_4' &= -\sum_{i=1}^N m_i \times \int_{\mathbb{R}^d} \phi(x) \Big(q_i \cdot W \frac{\partial \psi_i}{\partial q_i}(x) + H_i \cdot W \frac{\partial \psi_i}{\partial H_i}(x) \Big) dx \\ &= -\sum_{i=1}^N m_i \int_{\mathbb{R}^d} \phi(x) (Wx \cdot \nabla \psi_i) dx \\ &= -\int_{\mathbb{R}^d} \phi(x) (Wx \cdot \nabla \rho(x))\, dx.\end{aligned}$$

Using the first equation of (23) with $B = \mathrm{Id}$, L_4' becomes

$$\begin{aligned}L_4' &= -\int_{\mathbb{R}^d} \phi(x) (W \cdot \nabla \rho(x) x^T)\, dx \\ &= -W \cdot \int_{\mathbb{R}^d} \phi(x) \big(\nabla \rho(x) x^T \big)\, dx =: -W \cdot K.\end{aligned}$$

As it is shown below, the matrix K is symmetric and thus, $L_4' = 0$, because W is skew symmetric. To prove the symmetry of K we consider its entries $k_{ij}, i \neq j, i, j = 1, 2, \ldots, d$. Integration by parts yields

$$k_{ij} = \int_{\mathbb{R}^d} \phi(x) \frac{\partial \rho}{\partial x_i}(x) x_j\, dx = -\int_{\mathbb{R}^d} \frac{\partial \phi}{\partial x_i}(x) \rho(x) x_j\, dx$$

because of the compact support of ρ. For the symmetry of K we show that $k_{ij} - k_{ji}$ vanishes. With the potential $\phi(x) = \int_{\mathbb{R}^d} \Gamma(x-y)\rho(y)\, dy$ and because of $\Gamma(x-y) = g(|x-y|)$ we get

$$\begin{aligned}&k_{ij} - k_{ji} \\ &\quad = -\int_{\mathbb{R}^d} \frac{\partial}{\partial x_i} \Big\{ \int_{\mathbb{R}^d} \Gamma(x-y)\rho(y)\, dy \Big\} \rho(x)\, x_j\, dx \\ &\qquad + \int_{\mathbb{R}^d} \frac{\partial}{\partial x_j} \Big\{ \int_{\mathbb{R}^d} \Gamma(x-y)\rho(y)\, dy \Big\} \rho(x)\, x_i\, dx \\ &\quad = -\int_{\mathbb{R}^d} \int_{\mathbb{R}^d} g'(|x-y|) \frac{x_i - y_i}{|x-y|} \rho(y)\, \rho(x)\, x_j\, dy\, dx \\ &\qquad + \int_{\mathbb{R}^d} \int_{\mathbb{R}^d} g'(|x-y|) \frac{x_j - y_j}{|x-y|} \rho(y)\, \rho(x)\, x_i\, dy\, dx. \\ &\quad = \int_{\mathbb{R}^d} \int_{\mathbb{R}^d} g'(|x-y|) \frac{x_j y_i - x_i y_j}{|x-y|} \rho(y)\, \rho(x)\, dx\, dy\end{aligned}$$

Since the integrand is antisymmetric, the integral vanishes and thus, $k_{ij} - k_{ji} = 0$ holds and K is symmetric.

4 Semi-discrete model

The force terms involve integrals that can only be evaluated approximately in a computer code. This entails choosing appropriate quadrature rules.

[2] We write $A \cdot B = \mathrm{tr}(A^T B) = \sum_{i,j} a_{ij} b_{ij}$ for square matrices A and B.

4.1 Semi-discrete finite mass method

In order to compute the motion of the particles, the equations of motion (12) have to be solved. Therefore, the integrals of the forces have to be evaluated, and this should be done without disturbing the invariance of the particle model under translations and rotations. Since these properties are not conserved, if we use a quadrature formula with nodes fixed in space, the finite mass method uses a particle dependent quadrature formula for the approximation of the force integrals.

First, we explain the general approach to this quadrature formula before applying it to the integrals of internal pressure in (8). To this end, we consider an integral of the form $\int f\rho$. By inserting the mass density (3) and after transformation to the reference particle, we obtain

$$\int_{\mathbb{R}^d} f(x)\rho(x)\,dx = \sum_{i=1}^{N} m_i \int_{\mathbb{R}^d} f(q_i + H_i y)\psi(y)\,dy.$$

Again, $N \in \mathbb{N}$ denotes the number of particles. Now, it remains to evaluate these integrals on the support of the reference particle. To this end, the reference particle is equipped with quadrature points $a_\nu \in \mathbb{R}^d$ inside its support and weights $\alpha_\nu > 0$, $\nu = 1, 2, \ldots, n$. Note that the shape function ψ is used as weight function here and is already incorporated into the weights. In terms of individual particles this means that each particle i has its own quadrature points $X_\nu^i = q_i + H_i a_\nu$ and weights $\tilde{\alpha}_\nu^i = m_i \alpha_\nu$. These nodes are attached to the particle and move with it. Thus, the above integral can be approximated by the following sum

$$\begin{aligned}\int_{\mathbb{R}^d} f(x)\rho(x)\,dx &\to \sum_{i=1}^{N} m_i \sum_{\nu=1}^{n} \alpha_\nu f(q_i + H_i a_\nu) \\ &= \sum_{i,\nu} \tilde{\alpha}_\nu^i f(X_\nu^i) =: \int_{\mathbb{R}^d} f\,d\mu, \end{aligned} \tag{24}$$

i.e. the discrete integral $\int f\,d\mu$ can be evaluated by simply summing over all nodes of all particles.

By means of this quadrature formula we can define the discrete internal energy ($\tilde{\varepsilon} := \varepsilon/\rho$)

$$E_h^{\text{int}} = \int_{\mathbb{R}^d} \tilde{\varepsilon}(\rho, s)\,d\mu = \sum_{i=1}^{N} m_i \sum_{\nu=1}^{n} \alpha_\nu\, \tilde{\varepsilon}(q_i + H_i a_\nu),$$

Then, the pressure forces can be derived from the discrete energy analogously to the procedure in Sect. 2. Note that the pressure forces are not approximated by applying the quadrature rule directly to formula (8). Furthermore, by using this discrete internal energy the conservation properties of Sect. 2.4 carry over to the discrete situation (see [9, Sect. 3 and 4]).

4.2 Discrete gravitational fields

In the spirit of the previous section we have to introduce a discrete potential energy. Yet, we also have to worry about a discrete approximation ϕ_h of the potential ϕ. Both issues are settled instantly, once we fix a $H^1_{\text{loc}}(\mathbb{R}^d)$-conforming finite element trial space S_h for ϕ_h. It will be based on a grid G_h of a bounded domain $\Omega \subset \mathbb{R}^d$ with $\text{supp}(\rho) \subset \Omega$. For Ω large enough the error due to this cut-off will be arbitrarily small.

Using the weak form of the potential Eq. (17) we end up with: seek $\phi_h \in S_h$

$$a(\phi_h, \varphi_k) = (\rho, \varphi_k) \quad \text{for all } \varphi_k \in S_h, \tag{25}$$

with the scalar product

$$(u, v) := \int_\Omega u(x)\, v(x) dx \tag{26}$$

and the symmetric bilinear form

$$a(u, v) := -\int_\Omega \nabla u(x) \cdot \nabla v(x) dx.$$

Assuming problem (25) can be solved, the discrete potential ϕ_h is represented by the linear combination of (nodal) basis functions $\varphi_k \in S_h$

$$\phi_h = \sum_{k=1}^{m} \mu_k\, \varphi_k, \quad \mu_k \in \mathbb{R}, \tag{27}$$

where $m := \dim S_h$. We shortly write

$$\vec{\phi}_h = (\mu_k)_{k=1}^m \in \mathbb{R}^m,$$

where $\vec{\phi}_h$ denotes the coefficient vector of the discrete potential. With this representation of the potential ϕ_h, the gravitational energy required for the force computation becomes

$$E^{\text{pot}} = \frac{1}{2}\int_{\mathbb{R}^d} \phi_h(x)\rho(x)\,dx = \frac{1}{2}\sum_{k=1}^{m} \mu_k(\varphi_k, \rho). \tag{28}$$

However, neither (28) nor (25) is fully discrete, as the scalar product (26) still involves the exact evaluation of an integral. This is not possible, because the particle can have arbitrary position and orientation with respect to the finite element grid. The application of a quadrature rule is mandatory. In this case we have two possibilities to choose the quadrature formula:

- It could depend on the grid used for the approximation of the gravitational potential. This results in a quadrature formula which is fixed in space.
- It could depend on the particles like the quadrature rules introduced in Sect. 4.1.

By means of the discretised scalar product, the discrete potential can be computed, and we obtain a fully discrete representation of the gravitational energy. Finally, from this energy discrete gravitational forces are derived analogously to Sect. 3.

In the following we show how the gravitational forces are computed in each case. First, we have a look at the grid dependent quadrature rule used to approximate the scalar product (26).

4.3 The grid based quadrature

From now we fix S_h as a space of continuous multilinear functions on a non-uniform tensor product grid G_h. Such a grid can be considered as a hierarchy of increasingly finer tensor product grids which cover smaller and smaller subdomains. These grids may be extremely locally refined in such a way that the local grid size of abutting cells differs widely. However, a certain regular grid structure simplifies the algorithms. Thus, the construction we use will maintain local quasi-uniformity of the grid in the sense that the grid size of adjacent cells differs at most by the factor $\frac{1}{2}$.

To obtain a fully discrete representation of the right hand side of the variational formulation (25) as well as of the gravitational energy (28), we define a discrete counterpart of the scalar product (26). This discrete scalar product depends on the grid G_h: we start from a quadrature rule for each element e of G_h, which is characterised by quadrature points $p_i \in \mathbb{R}^d$ $(1 \le i \le n)$ and related weights $\omega_{p_i} \in \mathbb{R}$

$$\int_{\mathsf{e}} f(x)dx \to \sum_{i=1}^{n} \omega_{p_i} f(p_i).$$

Further, let $\mathcal{P}$ be the set of the quadrature points of all elements of G_h. Then, we can define a discrete scalar product independently of the particles by

$$(u, v)_G := \sum_{p\in\mathcal{P}} \omega_p u(p)v(p). \tag{29}$$

Now, we can discretise the right hand side of the variational Eq. (25)

$$a(\phi_h, \varphi_j) = (\rho, \varphi_j)_G \quad \forall\varphi_j,\ j = 1, 2, \ldots, m$$
$$\Leftrightarrow \textstyle\sum_{k=1}^{m} \mu_k a(\varphi_k, \varphi_j) = (\rho, \varphi_j)_G \quad \forall\varphi_j,\ j = 1, 2, \ldots, m.$$

We obtain the discrete Poisson equation

$$\Delta_h\vec{\phi}_h = \vec{\rho}$$

with the symmetric, negative definite stiffness matrix

$$\Delta_h := (a(\varphi_j, \varphi_k))_{j,k=1}^{m}$$

and the right hand side

$$\vec{\rho} := ((\rho, \varphi_k)_G)_{k=1}^{m}. \tag{30}$$

With this notation the discrete potential can now be written as solution of the discrete potential equation

$$\vec{\phi}_h = \Delta_h^{-1}\vec{\rho},$$

and thus, the coefficients μ_k have the representation

$$\mu_k = \sum_{j=1}^{m} \Delta_h^{-1}\Big|_{kj}\ \vec{\rho}_j = \sum_{j=1}^{m} \Delta_h^{-1}\Big|_{kj} (\rho, \varphi_j)_G. \tag{31}$$

In a straightforward fashion, based on the Euclidian scalar product $\langle ., .\rangle$ in $\mathbb{R}^m$, we define the discrete energy

$$E_h^{\mathrm{pot}} := \frac{1}{2}\langle\vec{\phi}_h, \vec{\rho}\rangle = \frac{1}{2}\sum_{k=1}^{m} \mu_k(\rho, \varphi_k)_G$$
$$= \frac{1}{2}\sum_{k=1}^{m} \mu_k \sum_{p\in\mathcal{P}} \omega_p \sum_{i=1}^{N} m_i\psi_i(p)\varphi_k(p). \tag{32}$$

This shows that definition (32) of the discrete potential energy is equivalent to replacing the scalar product in Eq. (28) by the discrete one (29).

By means of the discrete potential energy we can derive the gravitational forces analogously to the continuous case in Sect. 3. To compute the gravitational forces the derivatives of the potential energy (32) with respect to the positions q_i and the deformation matrices H_i of the particles are required. Here, we have

$$\frac{\partial}{\partial q_i} E_h^{\mathrm{pot}} = \frac{1}{2}\frac{\partial}{\partial q_i}\langle\vec{\phi}_h, \vec{\rho}\rangle = \frac{1}{2}\frac{\partial}{\partial q_i}\langle\Delta_h^{-1}\vec{\rho}, \vec{\rho}\rangle.$$

Using the symmetry of Δ_h^{-1} yields

$$\frac{\partial}{\partial q_i} E_h^{\mathrm{pot}} = \left\langle\Delta_h^{-1}\vec{\rho}, \frac{\partial}{\partial q_i}\vec{\rho}\right\rangle = \sum_{k=1}^{m} \mu_k \frac{\partial}{\partial q_i}(\varphi_k, \rho)_G.$$

Inserting

$$\frac{\partial}{\partial q_i}(\rho, \varphi_k)_G = \sum_{p\in\mathcal{P}} \omega_p \sum_{l=1}^{N} m_l \frac{\partial}{\partial q_i}\psi_l(p)\varphi_k(p)$$
$$= \sum_{p\in\mathcal{P}} \omega_p m_i \frac{\partial}{\partial q_i}\psi_i(p)\varphi_k(p),$$

we obtain

$$\frac{\partial}{\partial q_i} E_h^{\mathrm{pot}} = \sum_{k=1}^{m} \mu_k \sum_{p\in\mathcal{P}} \omega_p m_i \frac{\partial}{\partial q_i}\psi_i(p)\varphi_k(p).$$

Analogous computations for the deformation matrices lead to

$$\frac{\partial}{\partial H_i} E_h^{\mathrm{pot}} = \frac{1}{2}\frac{\partial}{\partial H_i}\langle\vec{\phi}_h, \vec{\rho}\rangle = \sum_{k=1}^{m} \mu_k \left(\varphi_k, \frac{\partial\rho}{\partial H_i}\right)_G$$
$$= \sum_{k=1}^{m} \mu_k \sum_{p\in\mathcal{P}} \omega_p m_i \frac{\partial\psi_i}{\partial H_i}(p)\varphi_k(p).$$

Finally, using (27) the formulas for the discrete gravitational forces are given by

$$F_i^{\mathrm{gr}} = -\frac{1}{m_i}\frac{\partial}{\partial q_i} E_h^{\mathrm{pot}} = -\sum_{p\in\mathcal{P}} \omega_p \frac{\partial\psi_i}{\partial q_i}(p)\phi_h(p),$$
$$M_i^{\mathrm{gr}} = -\frac{1}{m_i}\frac{\partial}{\partial H_i} E_h^{\mathrm{pot}} = -\sum_{p\in\mathcal{P}} \omega_p \frac{\partial\psi_i}{\partial H_i}(p)\phi_h(p). \tag{33}$$

4.4 The particle based quadrature

As an alternative to the grid based quadrature formula we can use a particle based quadrature formula to discretise the scalar product on the right hand side of the variational formulation (25). Then again, by means of this discrete scalar product we obtain a fully discrete representation of the potential energy (28) from which the discrete gravitational forces can be derived. To define the discrete scalar product

corresponding to (26), we use the quadrature formula (24) of Sect. 4.1. As one argument will always be the mass density ρ, we can set

$$(\rho, v)_P := \sum_{i=1}^{N} m_i \sum_{\nu=1}^{n} \alpha_\nu v(q_i + H_i a_\nu) = \sum_{i,\nu} \tilde{\alpha}_\nu^i v\big(X_\nu^i\big).$$

Then, the variational formulation of the potential equation is given by

$$a(\phi_h, \varphi_k) = (\rho, \varphi_k)_P \quad \text{for } \varphi_k \in S_h, \quad k = 1, 2, \ldots, m$$

with the discrete right hand side

$$\begin{aligned}(\rho, \varphi_k)_P &= \sum_{i=1}^{N} m_i \sum_{\nu=1}^{n} \alpha_\nu \varphi_k(q_i + H_i a_\nu) \\ &= \sum_{i,\nu} \tilde{\alpha}_\nu^i \varphi_k\big(X_\nu^i\big).\end{aligned} \tag{34}$$

Thus, we get the discrete Poisson equation $\Delta_h \vec{\phi}_h = \vec{\rho}$, with a right hand side arising from the particle based scalar product $\vec{\rho} := ((\rho, \varphi_k)_P)_{k=1}^m$. The discrete potential $\vec{\phi}_h = \Delta_h^{-1} \vec{\rho}$ can be represented as in (31) now using the particle based scalar product.

Analogously to the preceding section we can define the discrete potential energy as

$$E_h^{\text{pot}} := \frac{1}{2} \langle \vec{\phi}_h, \vec{\rho} \rangle = \frac{1}{2} \sum_{k=1}^{m} \mu_k (\varphi_k, \rho)_P.$$

Thus, for the discrete potential energy we obtain a formula depending on the particle quadrature points. Again, this definition is equivalent to replacing the term of the scalar product in Eq. (28) by the discrete one (34).

If we assume for the moment that the basis functions φ_k are continuosly differentiable, the discrete gravitational forces acting upon the particles can be derived as before from the given discrete potential energy E_h^{pot} and are again

$$\frac{\partial}{\partial q_i} E_h^{\text{pot}} = \frac{1}{2} \frac{\partial}{\partial q_i} \langle \vec{\phi}_h, \vec{\rho} \rangle = \sum_{k=1}^{m} \mu_k \frac{\partial}{\partial q_i} (\rho, \varphi_k)_P.$$

Inserting (34) yields

$$\begin{aligned}\frac{\partial}{\partial q_i} E_h^{\text{pot}} &= \sum_{k=1}^{m} \mu_k \sum_{j=1}^{N} m_j \sum_{\nu=1}^{n} \alpha_\nu \frac{\partial}{\partial q_i} \varphi_k(q_j + H_j a_\nu) \\ &= m_i \sum_{\nu=1}^{n} \alpha_\nu \sum_{k=1}^{m} \mu_k \frac{\partial}{\partial q_i} \varphi_k(q_i + H_i a_\nu).\end{aligned}$$

With analogous computations for the derivatives with respect to H_i we obtain the representation

$$\begin{aligned}F_i^{\text{gr}} &= -\textstyle\sum_{\nu=1}^{n} \alpha_\nu (\nabla \phi_h)(q_i + H_i a_\nu), \\ M_i^{\text{gr}} &= -\textstyle\sum_{\nu=1}^{n} \alpha_\nu [(\nabla \phi_h)(q_i + H_i a_\nu)][a_\nu]^T.\end{aligned} \tag{35}$$

Remark. Unfortunately, the standard multilinear trial functions are not sufficiently smooth to allow for these operations. However, as shown by the examples below, the method nevertheless works well, if one formally adopts the expressions above and simply replaces the discontinuous gradient $\nabla \phi_h$ with the continuous multilinear interpolant of an averaged $\nabla \phi_h$. This technique was used throughout in the numerical experiments that employed particle based quadrature.

4.5 Conservation properties

Deriving the equations of motion from a discrete Lagrangian involves the conservation of the total discrete energy, as long as we use a trial space S_h that does not vary with time.

Theorem 3 *The discrete energy*

$$E_h^{\text{tot}}(t) := E^{\text{kin}}(t) + E_h^{\text{int}}(t) + E_h^{\text{pot}}(t)$$

is conserved.

Proof The usual techniques, cf. the proof of Theorem. 2, carry over to the discrete setting, see [2, Sect. 3.2.3].

However, employing an Eulerian grid rules out the invariance of the model with respect to translations and rotations. Thus, we can no longer expect the conservation of total (discrete) linear and angular momentum, as it is guaranteed for the plain finite mass method described in Sects. 2 and 4.1, respectively.

Remark. In the case of the particle dependent quadrature, the proved conservation of the energy holds only if the forces (35) use the true potential gradient $\nabla \phi_h$. If force computation relies on a smoothed gradient, the conservation of total discrete energy does not hold anymore. However, the computational experiments of Sect. 6 show that the conservation of the total energy seems not to be affected much by employing a smoothed gradient. This seems to be a good way to improve the accuracy of the method with minimal impact on the conservation of the energy.

Remark. The two options for the discretisation of the scalar product (26) can be combined: it can be advantageous to use the grid based quadrature to evaluate the right hand side of the discrete potential equation (cf. formula (30)) and to apply the particle based quadrature to the computation of the force integrals (cf. formula (35)), as we will discuss at the end of Sect. 5. Yet, a strict conservation of energy remains elusive in this case.

5 Aspects of implementation

5.1 Pressure forces

Forces constitute the right hand side of the large system of ordinary differential equations describing the evolution of particles and fields. Their computation is a core algorithmic issue. Let us recall the strategy for the computation of the pressure forces [9, 15]: The crucial distinction is between

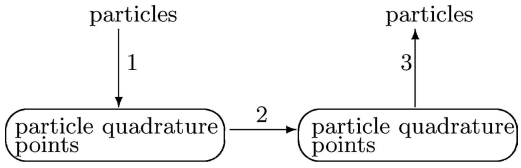

Fig. 2 Computation of the discrete force integrals of internal pressure

data associated with particles (like m_i, S_i, q_i, H_i, q_i', and H_i'), and data required at the particle quadrature points like ρ, s, $\frac{\partial\tilde{\varepsilon}}{\partial\rho}$, and $\frac{\partial\tilde{\varepsilon}}{\partial s}$. These are kept in independent data structures.

The computation of the first term of the internal pressure forces proceeds as schematically shown in Fig. 2:

1. Interpolate the required particle data (ρ, s) at the particle quadrature points X_v^i
2. Compute $\frac{\partial\tilde{\varepsilon}}{\partial\rho}$ and $\frac{\partial\tilde{\varepsilon}}{\partial s}$ required for the forces at the quadrature points X_v^i
3. Evaluate the discrete force integrals

5.2 Gravitational forces

As the discrete potential ϕ_h is given as a finite element function on a grid, the transfer of information between grid and particles becomes a key issue. In Sect. 4.3 and 4.4 we outlined how it can be accomplished using different quadrature policies. Figure 3 shows a schematic diagram of the force computation procedure independent of the applied quadrature rule that proceeds as follows:

1. Computation of the right hand side of the discrete potential equation, i.e. the evaluation of the discrete scalar product $(.,.)_G$ or $(.,.)_P$
2. Computation of the gravitational potential (e.g. by a multigrid method)
3. Computation of the forces, i.e. evaluation of (33) or (35)

5.2.1 Grid based quadrature

In this case, to approximate the potential, the right hand side (30) of the discrete Poisson equation has to be computed first by means of the discrete scalar product (29). The storage of the values of the mass density at the quadrature points is essential to save computational effort. To this end, the mass density ρ has to be interpolated at the quadrature points of the grid. Again, we use the fact, that the mass distribution functions ψ_i of the particles have compact support. Hence, for the density value at a quadrature point w we have to consider only the particles ψ_i fulfilling $w \in \mathrm{supp}\,(\psi_i)$

$$\rho(w) = \sum_{i,\, p\in\mathrm{supp}(\psi_i)} m_i \psi_i(w).$$

In order to avoid traversing the particle set for each quadrature point, we evaluate this sum by distributing the density contributions of the particles to the values at the quadrature points. Therefore, we have to find all quadrature points contained in a particle. This is done by searching the grid cells intersecting a particle, i.e. the support of ψ_i. These elements and, thus, the quadrature points contained in the support of a particle can be easily determined by using the bounding box of each particle (i.e. the smallest rectangle with edges parallel to the axes containing the particle).

For the computation of the right hand side of the potential equation, i.e. the discrete scalar product, a loop over all quadrature points is required during which the values at the quadrature points are distributed to the vector components $(\vec{\rho})_k$.

After the interpolation of the mass density and the evaluation of the discrete scalar product, the potential equation can be solved, e.g. by a multigrid method. Then, the gravitational potential is given at the grid points. To compute the forces (cf. Eq. (33)) the potential is required at the quadrature points where it has to be interpolated. It can also be useful to store these values because the nodes can be contained in the supports of several particles and thus, they contribute to the forces of each of these particles. As before we can exploit that ψ_i and φ_k have compact support. Hence, the interpolation of the potential is given by

$$\phi_h(w) = \sum_{\substack{k=1 \\ p\in\mathrm{supp}(\varphi_k)}}^{m} \mu_k \varphi_k(p),$$

and formula (33) for the force computation reduces to

$$F_i^{\mathrm{gr}} = -\sum_{\substack{p\in\mathcal{P} \\ w\in\mathrm{supp}(\psi_i)}} \omega_p \frac{\partial\psi_i}{\partial q_i}(p) \sum_{\substack{k=1 \\ p\in\mathrm{supp}(\varphi_k)}}^{m} \mu_k \varphi_k(p),$$

$$M_i^{\mathrm{gr}} = -\sum_{\substack{p\in\mathcal{P} \\ w\in\mathrm{supp}(\psi_i)}} \omega_p \frac{\partial\psi_i}{\partial H_i}(p) \sum_{\substack{k=1 \\ p\in\mathrm{supp}(\varphi_k)}}^{m} \mu_k \varphi_k(p).$$

Hence, also the force computation involves a loop over all particles.

Particle based quadrature

If this strategy is used for the computation of the gravitational forces, the particle data are required at the particle quadrature points. However, this interpolation procedure is already done for the computation of the pressure forces. Largely, it is the same as for the grid quadrature points and

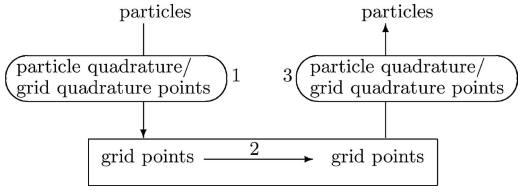

Fig. 3 Computation of the gravitational force

can be done by a loop over all particles. For the computation of the right hand side (34) basically the weights $\tilde{\alpha}_\nu^i = m_i \alpha_\nu$ of the particle quadrature points are required. But they can be computed once and for all because the particles do not change their mass, and the weights and the locations of the quadrature points are fixed with respect to the particle. Then, the evaluation of (34) consists of a loop over all particle quadrature points. To this end, the element of the grid containing a particle quadrature point has to be found.

After the approximation of the potential, the gradient of the potential has to be interpolated at the particle quadrature points. Since the gradient of the potential is required only once at each particle quadrature point, its value need not be stored.

Remark. Thanks to the simple tensor product structure of the grid, see Sect. 4.3, it takes simple index calculations to determine the grid cells, in which a point is located.

5.3 Grids and adaptivity

There are many rationales for using a non-uniform and temporally varying grid G_h for the computation of the discrete potential ϕ_h:

- the mass distribution may be grossly non-uniform and display considerable temporal variations.
- the artificial boundary of the computational domain has to be sufficiently far from $\mathrm{supp}\rho$ to justify the use of a simple boundary condition (as, e.g., (36) in Sect. 6). Thus, it may have to be extended, if ρ changes.
- far off $\mathrm{supp}\rho$ the potential will be very smooth and can be economically resolved on a rather coarse grid.
- in order to guarantee a prescribed accuracy of the finite element solution grid adaptation controlled by an a-posteriori error estimator must be applied [6].

It turns out that the quadrature policy – the grid based as well as the particle based – has a profound impact on the grid refinement strategy:

Grid based quadrature: the grid refinement has to guarantee that the support of each particle contains at least a few grid quadrature points. If this rule is ignored, a particle not containing any grid quadrature points would not give a contribution to the right hand side of the potential equation and would not be influenced by the gravitational force. As particles can shrink significantly, a substantial part of the mass can become invisible to the potential equation. The need for the grid to resolve small particles can lead to excessive grid refinement and can clash with control by an a-posteriori error estimator.

Particle based quadrature: the refinement of the grid has to guarantee that particle quadrature points are contained in each element of the grid intersected by a particle. Otherwise some grid cells will fail to see any mass density. This will be mistaken for strong oscillations of the right hand side by an error estimator and lead it astray. Thus, the grid resolution has a lower bound given by the particle size. However, this is not very satisfactory, since for a good approximation of the potential and particularly, of the gradient of the potential, a finer grid may be necessary.

Summing up, with both methods a coupling of the grid refinement with the particle size is necessary. This is not the case with the asymmetric quadrature policy sketched at the end of Sect. 4.5, which uses the grid based quadrature for the evaluation of the right hand side scalar product (cf. Eq. (30)) and the particle based quadrature for the force computation (cf. Eq. (35)). The advantage of this procedure is that the refinement of the grid is largely independent of the particles and thus, an error estimator can be applied easily. Yet, there is no theory which ensures the conservation of energy. However, if the approximation of the respective integrals is good enough, this may be negligible.

5.4 Computational effort

A crude estimate for the computational effort involved in the transfer of information between particles and grid can be obtained by counting the number of accesses to quadrature points.

Below, let N denote the number of particles, n^P the total number of particle quadrature points, and n_i^P the number of particle quadrature points contained in the support of the ith particle. Analogously, let n^G denote the total number of grid quadrature points and n_i^G the number of grid quadrature points contained in the support of the ith particle. With these notations Table 1 summarises the following consideration.

First, we consider the interpolation of the mass density at the quadrature points (cf. Table 1, Step 1). For this interpolation a particle contributes to the density at each quadrature point it contains. Therefore, using the particle oriented method, the effort depends on $\sum_{i=1}^N n_i^P$. Note that the interpolation at the particle quadrature points is also required for the computation of the pressure forces and thus, this means no additional effort. Applying the grid oriented or asymmetric method, the effort for the interpolation depends on $\sum_{i=1}^N n_i^G$.

For the computation of the right hand side of the discrete potential equation, we only have to consider the effort for

Table 1 Dependence on the number of quadrature points of the computational effort

Method	Particle oriented	Asymmetric	Grid oriented
1. Interpolation of ρ	$\sum_{i=1}^N n_i^P$	$\sum_{i=1}^N n_i^G$	
2. Right hand side: quadrature	n^P	n^G	
restriction	Same effort for same grids		
3. Multigrid method	Same effort for same grids		
4. Force computation:			
(a) Interpolation of $\nabla\phi_h$, resp. ϕ_h	n^P		n^G
	(+ effort for smoothing $\nabla\phi_h$)		
(b) Forces of the particles	n^P		$\sum_{i=1}^N n_i^G$

the evaluation of the quadrature rule on the individual grid elements. Hence, the costs of the quadrature depend on the total number of quadrature points, i.e. on n^P using the particle oriented method and n^G using the grid oriented method and thus, also using the asymmetric method (cf. Table 1, Step 2).

Next, for the force computation the potential (grid based method) or the gradient of the potential (particle based and asymmetric method) has to be interpolated at the respective quadrature points (cf. Table 1, Step 4(a)). If these values are stored, the costs are proportional to n^G and n^P, respectively. Smoothing of the gradient requires additional work.

Finally, the effort for the evaluation of the forces depends on n^P in the case of the particle based and asymmetric method, since only the quadrature points of the ith particle contribute to the forces acting on this particle. Therefore, in this case one need not store the values of the gradient of the potential at the quadrature points. Conversely, using the grid based method, a grid quadrature point contributes to the forces of all particles in which it is contained. For this reason, the effort for the force computation depends on $\sum_{i=1}^{N} n_i^G$ (cf. Table 1, Step 4(b)). Furthermore, if the values of the potential are not stored at the quadrature points, the interpolation of the potential has to be carried out many times.

One advantage of the particle oriented method is that the interpolation of the density is also required for other force computations and thus, causes no additional effort. Moreover, the evaluation of the gravitational forces acting on the ith particle only depends on its quadrature points. The same is true of asymmetric method. However, using these methods in practice entails smoothing the gradient of the potential, which means additional costs.

6 Numerical experiments

We study the behaviour of the finite mass mesh method for a few two-dimensional cases. This can be thought of as a three-dimensional arrangement with translation invariance in one coordinate direction. In a sense, we look at the evolution of "gas columns" under self-gravity. For all examples the equation of state of barytropic ideal gases

$$\varepsilon = \frac{\pi_0}{\gamma - 1} \left(\frac{\rho}{\rho_0} \right)^{\gamma} \exp\left(\frac{s}{c_v \rho} \right)$$

with $\rho_0 = 1$, $\pi_0 = \frac{\gamma-1}{\gamma}$, and $\gamma = 1.4$ provides the density of the internal energy which is required e.g. for the computation of the pressure forces. In all examples the pressure forces, the gravitational forces, the frictional forces, and the heat production are taken into account. Throughout scaled equations are considered.

The gravitational potential is computed on a non-uniform tensor product grid using continuous piecewise bilinear finite elements. We remark that in our computations on the boundary of the cut-off domain Ω (cf. Sect. 4.2) the Dirichlet boundary conditions

$$\phi(x) = \sum_{i=1}^{N} m_i \frac{1}{2\pi} \log(|x - q_i|), \quad x \in \partial\Omega \tag{36}$$

are imposed. This amounts to an approximation of the particles by point masses. If the boundary of Ω is far enough away from the boundary of the support of ρ, this assumption is reasonable.

The discrete potential equation is solved by means of a hierarchical transformation multigrid method (s. [10]), which enjoys fast convergence such that its truncation error is negligible, by and large. If the force terms are evaluated by the particle based quadrature rule, the potential gradient has to be smoothed. In all two-dimensional numerical tests this is achieved by averaging at the grid points and subsequent bilinear interpolation.

For the particle based quadrature strategy of Sect. 4.1 the quadrature rule described in [9, Sect. 4] is used. This quadrature formula is exact for fifth order polynomials, and in this approach a particle owns 25 quadrature points. For the grid based quadrature, the tensor product of a one-dimensional three point Gauß quadrature rule is used. An exponential integrator is used for timestepping, cf. [9, Sect. 5], [13].

Since the method does not prevent the particles from large deformations, they can become thin long "needles" that are not capable of adapting properly to the curvature of a flow. Of course, as long as integration in time is done exactly this does not affect stability: since the energy is conserved and therefore bounded, the particles cannot become arbitrarily small in a finite time interval. But in the fully discrete setting this could mean a tight threshold on the size of the time steps.

To overcome these problems we use *restarts* of the simulation. If the size of a particle decreases too much, the current particle set is discarded and the global physical quantities, like the mass density and the velocity field, are represented by a new set of particles. This restart method was presented and analysed in [8], to which we refer for more details. We point out that more elaborate restarting schemes are conceivable [16], but they had not yet been implemented at the time of our numerical experiments. Restarts are related to the projections used in almost all solution methods for conservation laws. However, in contrast to these methods that use such interpolations in every time step, in the finite mass method the restart is employed more rarely.

For the approximation of the initial data, we proceed as described in [9, Sect. 6]. As a result, we obtain an initial particle configuration which is arranged on a regular grid covering the region occupied by mass.

6.1 Gas column in hydrostatic equilibrium

For this first numerical example we have an analytic solution (exact scaled radius 3.229). The discretisation by the finite mass method relies on 1041 particles and the problem is

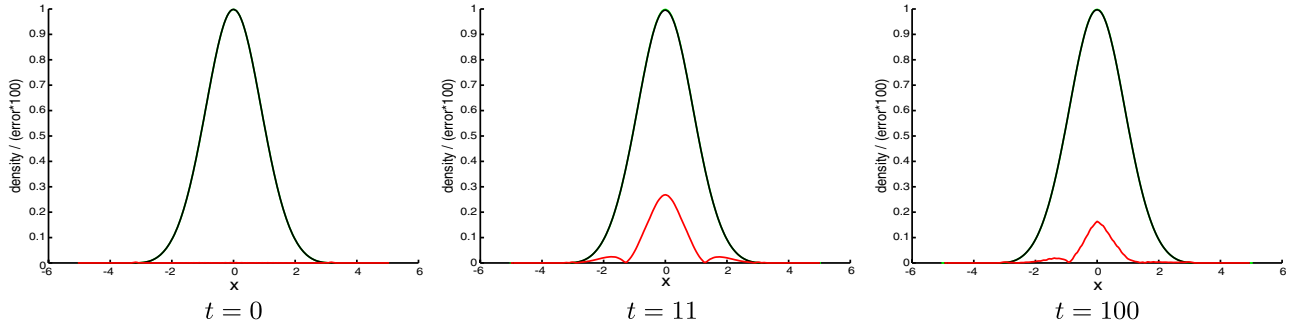

Fig. 4 Cross sections of the mass density and the corresponding error (scaled by 100 and plotted in red) of the gas column in equilibrium at time t (bilinearly interpolated averaged gradient of potential)

solved for the period $0 \leq t \leq 101$ by an exponential integrator using 10100 time steps. [3] The potential is approximated on a non-uniform tensor product grid which is adapted by a hierarchical a-posteriori error estimator. This is feasible, because the asymmetric quadrature policy is used, which permits us to decouple the grid resolution from the particle size.

The approximate solution for ρ is compared with the exact equilibrium density. In Fig. 4, one-dimensional cross sections along the x-axis of the approximated density and the error (plotted in red and multiplied by the factor 100) are depicted. We observe an oscillation of the error which indicates that the approximation oscillates slightly around the equilibrium state. But the difference of the exact and the approximated density is rather small.

6.2 Rotating and oscillating gas column

For this example we use the transformed initial mass density $\rho(r) := c^2 \cdot \hat{\rho}(c\,r)$, where $\hat{\rho}(r)$ denotes the density corresponding to the equilibrium state of the previous example and $c = 0.85$. Moreover, the gas column is provided with the angular velocity $\omega = 0.1$. This yields a configuration of a rotating gas column that is not in equilibrium but oscillates around the equilibrium state. Again, for the simulation 717 particles, and 10100 time steps on the time interval [0, 101] are used. First, we show results for the particle based method. The refinement of the grid is controlled by the particle size.

The particle configuration in Fig. 7 illustrates alternating phases of contraction (e.g. $t = 0,\ 4,\ 6$) and expansion (e.g. $t = 8,\ 12,\ 14$). In Fig. 7 one particle is marked to follow the motion. One can observe the rotation of the gas column, its contraction, and expansion. The regular orientation of the particles is conserved during the motion.

The total angular momentum is shown in Fig. 5. The relative change of the angular momentum remains in the range of $2 \cdot 10^{-4}$. We remark that the oscillations of the angular momentum seems to be an effect of the change of the grid that is adapted to the current particle distribution.

[3] Unless mentioned otherwise, frictional forces are computed with $R = 500$, see [9].

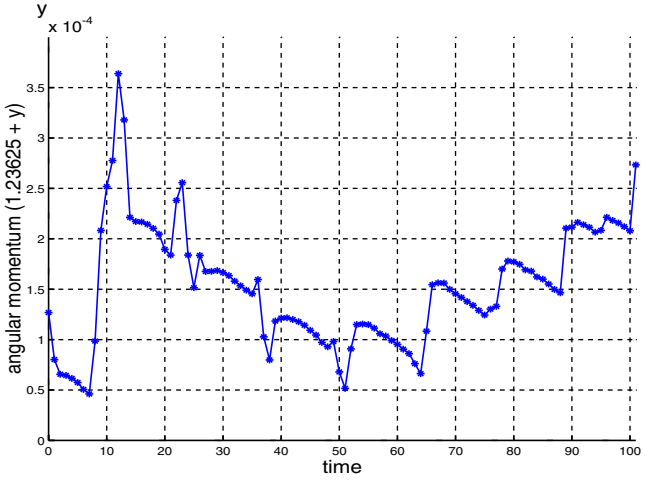

Fig. 5 Total angular momentum of the rotating and oscillating gas column and its relative change (note that for the actual value of the angular momentum one has to add the value 1.23625)

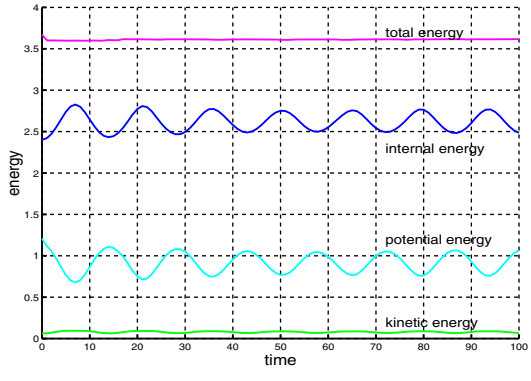

Fig. 6 Energy balance in the case of the rotating and oscillating gas column (particle oriented method)

The energy balance shown in Fig. 6 illustrates the alternative transformation of the individual energies corresponding to the oscillation. The total energy is conserved. The oscillations are slightly damped which is an effect of the friction (artificial viscosity).

For comparison, we conduct this simulation also with the asymmetric method. The simulation basically behaves alike.

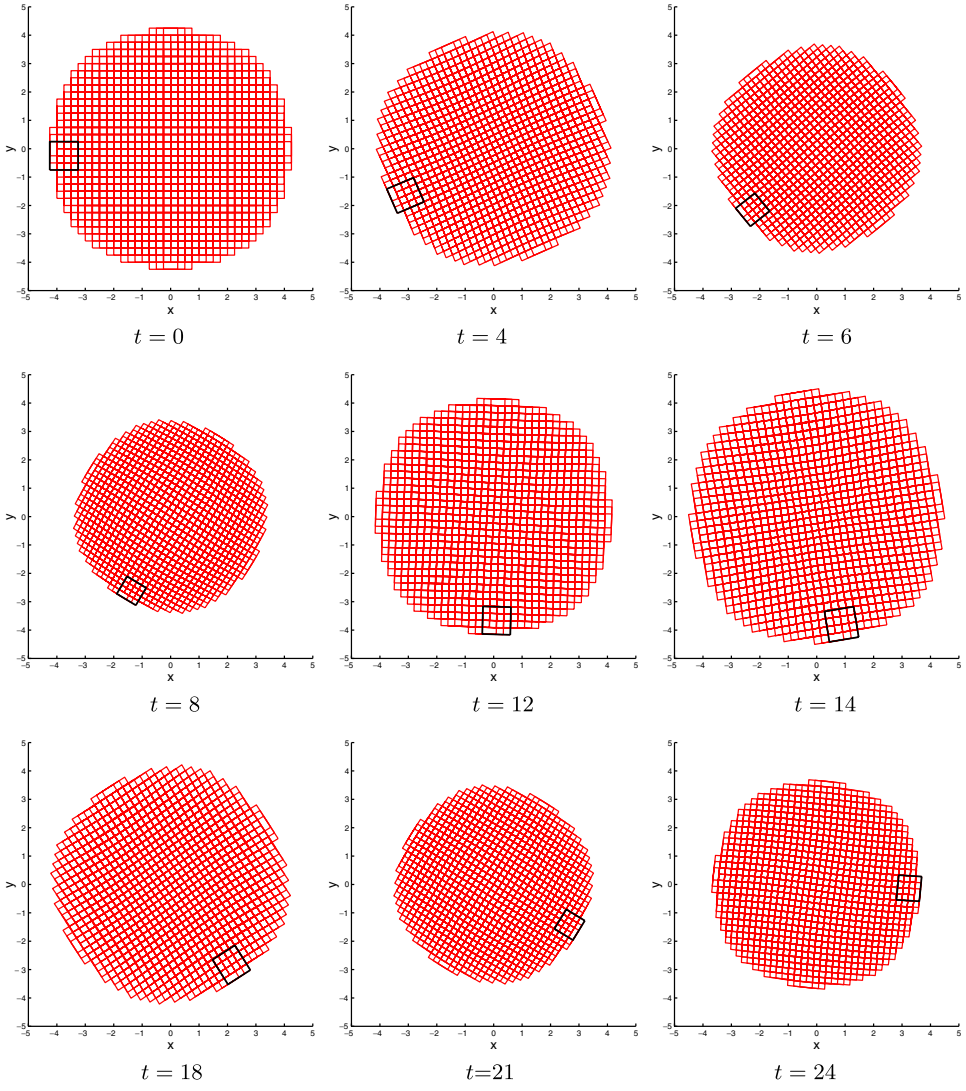

Fig. 7 Particles of the two-dimensional rotating and oscillating gas column at time t

The plot of Fig. 8 shows the energy balance in a simulation applying the asymmetric method. The energy balance seems to be unchanged. Thus, the asymmetric method does not disturb the conservation of energy. Also the range of the relative change of the total angular momentum is the same as before.

6.3 Two-dimensional colliding gas columns

The following numerical examples examine gas columns in equilibrium attracting each other by gravitation. Eventually, they collide, merge and oscillate around an equilibrium state.

When the gas columns collide, strong forces due to friction act on the particles. First of all the particles at the boundary of the gas columns, which have small masses, deform strongly. As explained earlier, this enforces restarts triggered by shrinking particles. The criterion for a restart is

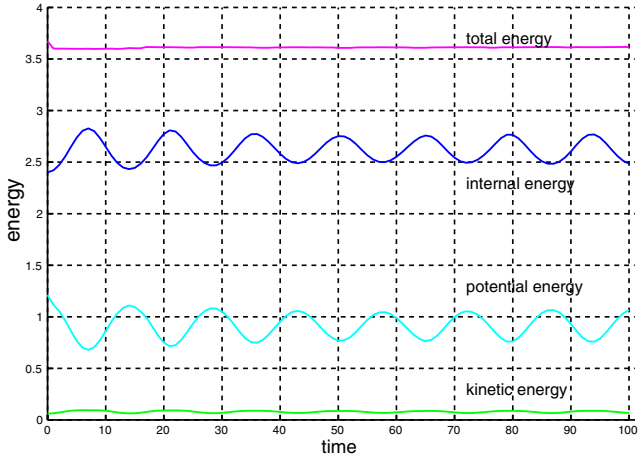

Fig. 8 Energy balance in the case of the rotating and oscillating gas column (asymmetric method)

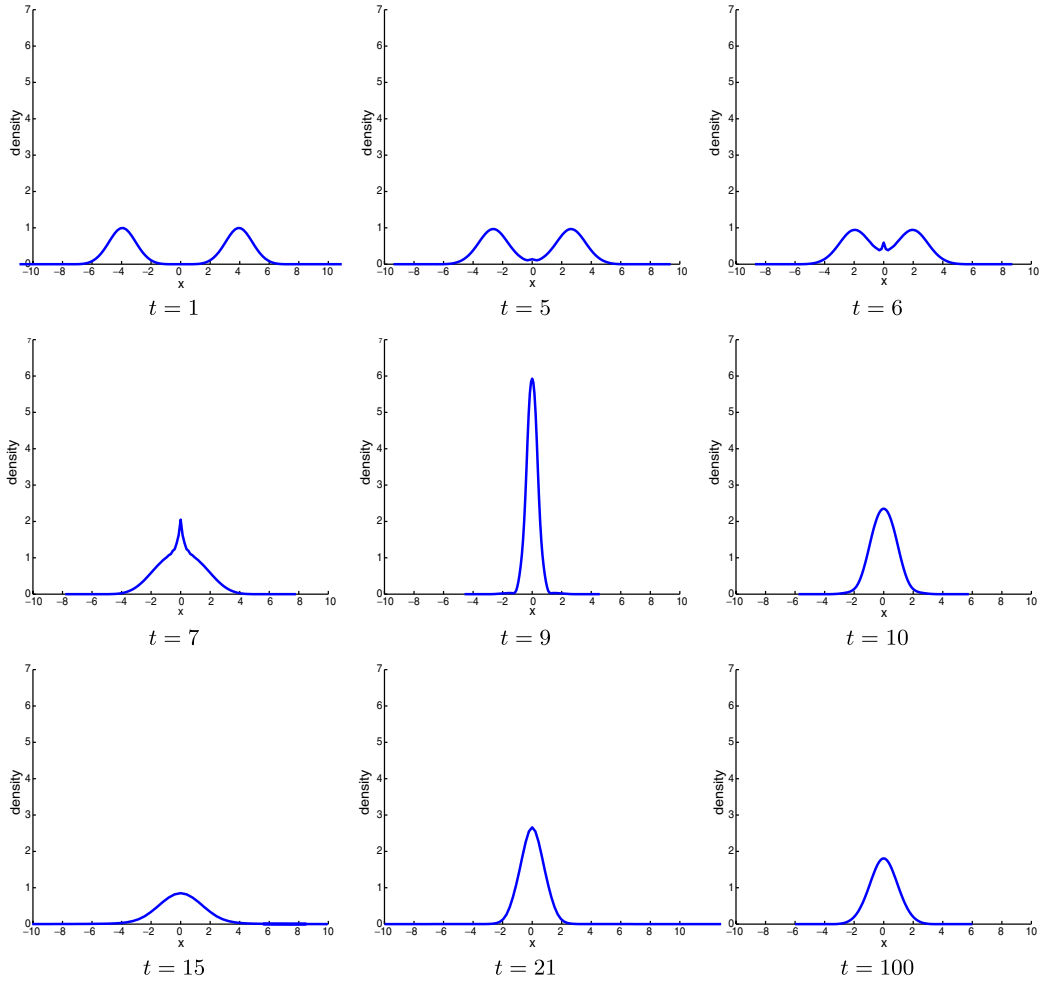

Fig. 9 Cross sections of the mass density in the case of two two-dimensional gas columns attracting each other at time t

the change of the particle size, particularly the change of the determinant of the deformation matrices H_i. For the simulation, the time interval [0, 101] is considered, and 10100 time steps and 89 restarts are used (cf. Fig. 10).

The computation starts with 966 particles, and the initial gas columns are given by the mass density of the example of Sect. 6.1 and their centres are located on the x-axis 8 distance units apart. [4] Again, the asymmetric method is applied for the computation of the gravitational forces and the grid refinement is coupled with the particle size.

In Fig. 9 cross sections of the mass density along the x-axis are shown. The gas columns attract each other by the gravitational forces ($t = 1$), penetrate each other ($t = 5$), merge ($t = 7$), and begin to oscillate ($t > 9$). For illustration also some two-dimensional plots of the density are presented in Fig. 12.

The corresponding particle sets are shown in Fig. 11. One can observe that the particles deform in the area where the columns begin to penetrate ($t = 5, 6, 7$). Note that because of the restarts the particles are not deformed very

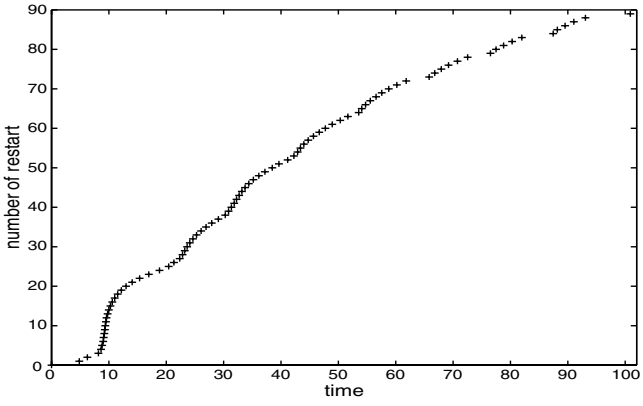

Fig. 10 Restarts of the simulation of two gas columns attracting each other

[4] This time, the friction parameter R is chosen as function depending on the density ($R = 500\rho$), see [9]. This implies that the frictional forces are smaller at the boundary of the gas columns where they penetrate first and increase with the increasing mass density during the collision.

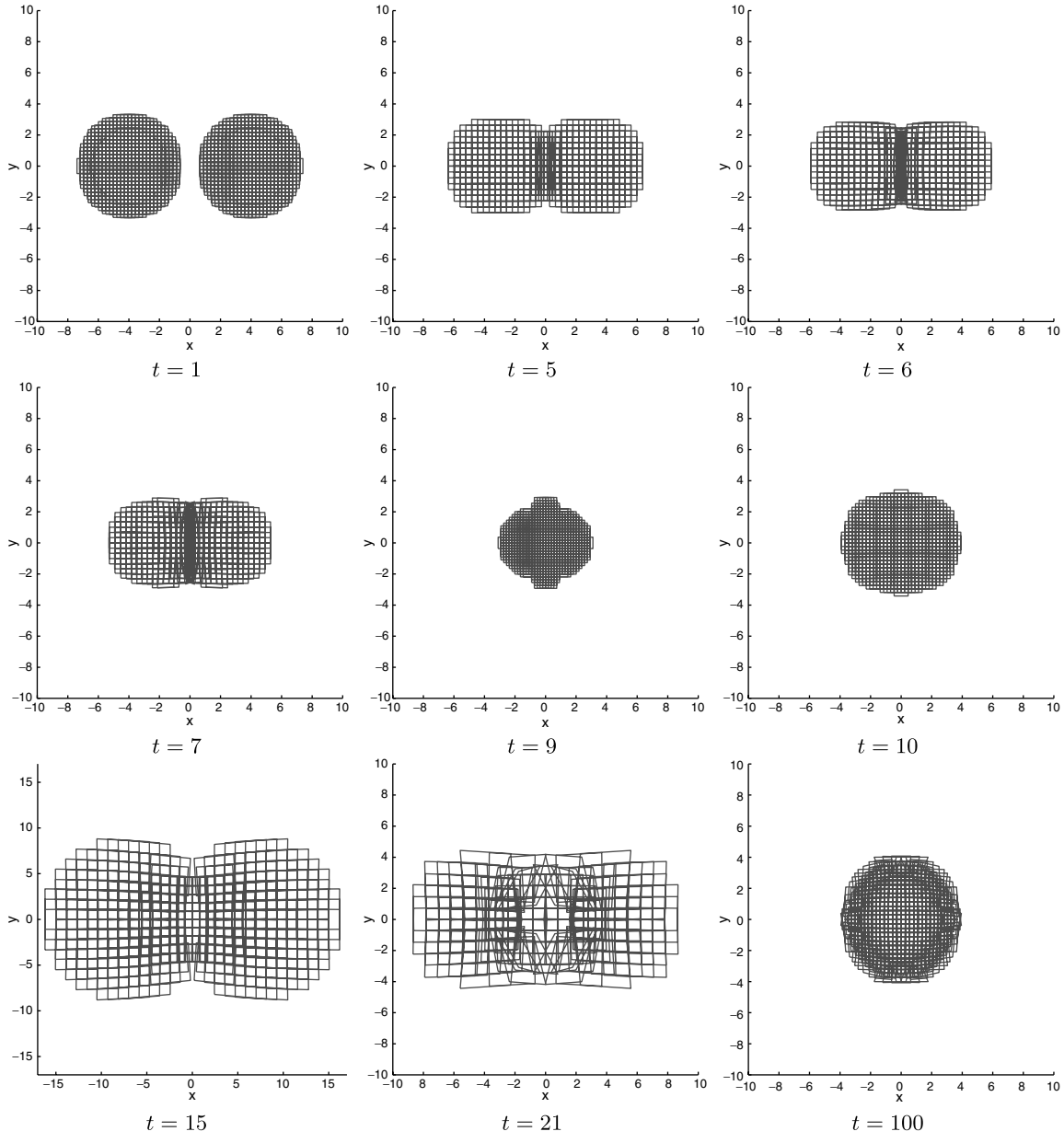

Fig. 11 Particles of two gas columns attracting each other at time t (note that in the diagram at time $t = 15$ the scale is changed)

strongly and the number of the particles changes during the simulation. At the time $t = 100$, the orientation of the particles are similar to the one we have seen in the example of the gas column in equilibrium. Mainly the particles at the boundary of the column deform, whereas in the interior the regular orientation is conserved. This seems to indicate that the configuration becomes stable.

The details of some grids used for the computation of the gravitational potential are shown in Fig. 13. During the collision the grid can contain much more elements than in the grids presented here, e.g. 21120 squares at the time $t = 9$. For comparison, the grids for the same experiment, now controlled by the error estimator are shown in Fig. 14. These grids are much smaller.

The restart scheme we use conserves the total mass and the total entropy. Considering the energy balance (s. Fig. 15) we observe that the total energy shows some oscillations as well as the potential energy. Since the discrete potential energy depends on the grid this is not surprising. If the program is restarted the grid has to be built anew from the new particle data. This may change the grid and the grid data more than the adaptation of the grid in each time step. In addition, the decrease of the total energy at the time of the collision can be an effect of the time discretisation. However, Fig. 15 also shows that the energy is basically conserved. First, the gravitational energy decreases since the gas columns are accelerated due to the gravitation. Thus, the kinetic energy increases. The internal energy mainly remains

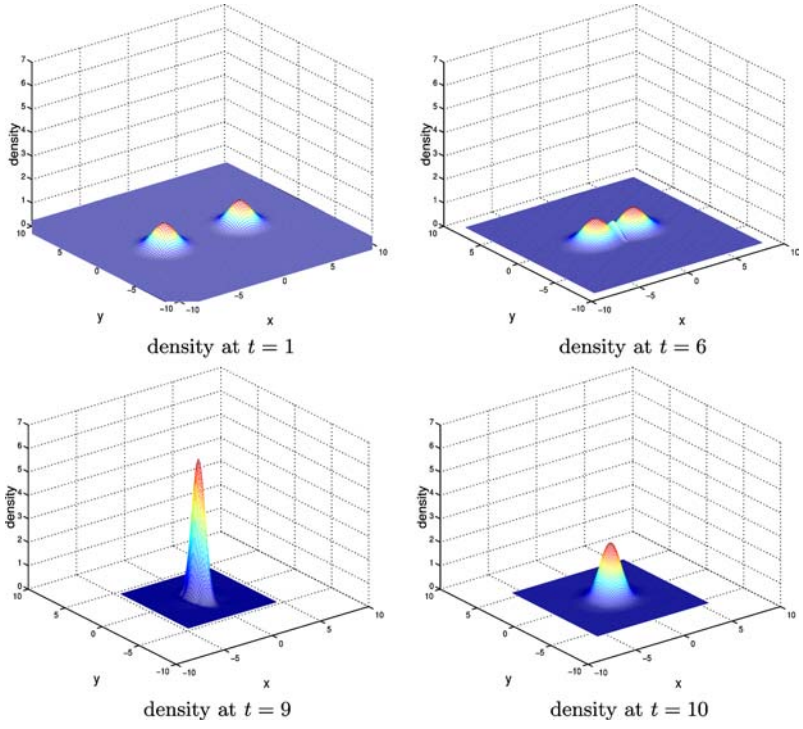

Fig. 12 Mass density of two gas columns attracting each other at time t

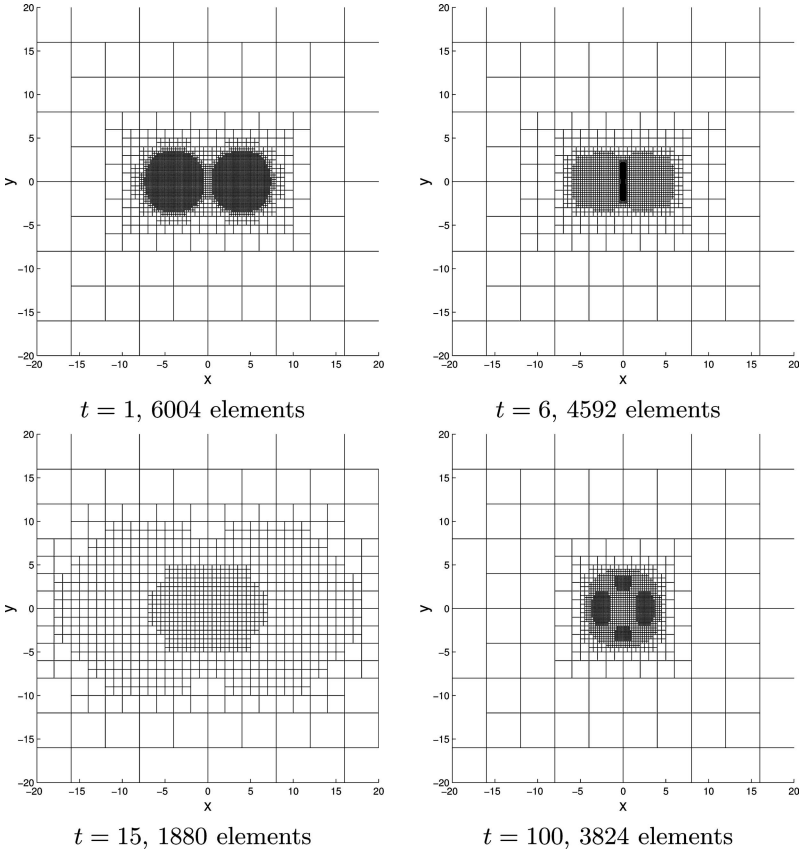

Fig. 13 Grids in the case of two gas columns attracting each other at time t (particle based refinement)

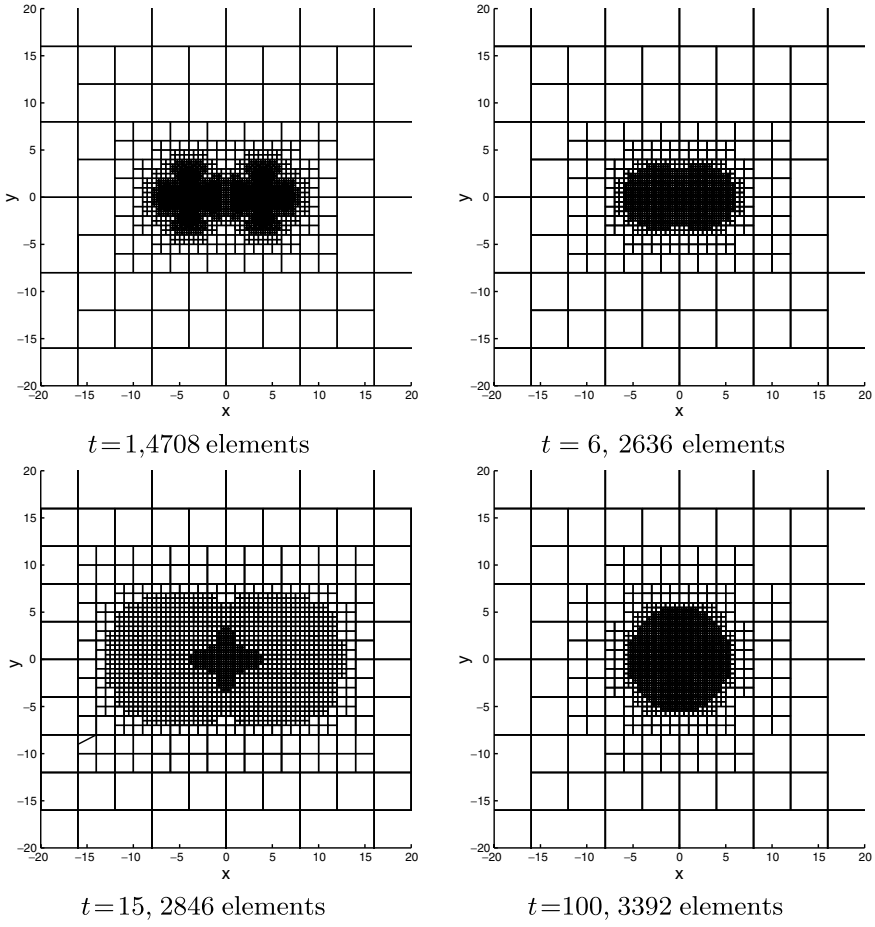

Fig. 14 Grids controlled by the error estimator in the case of two two-dimensional gas columns attracting each other at time t

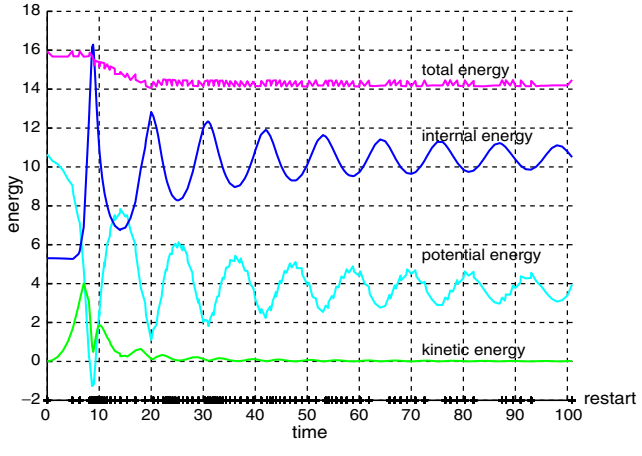

Fig. 15 Energy balance in the case of two attracting two-dimensional gas columns (with marked restarts on the time axis)

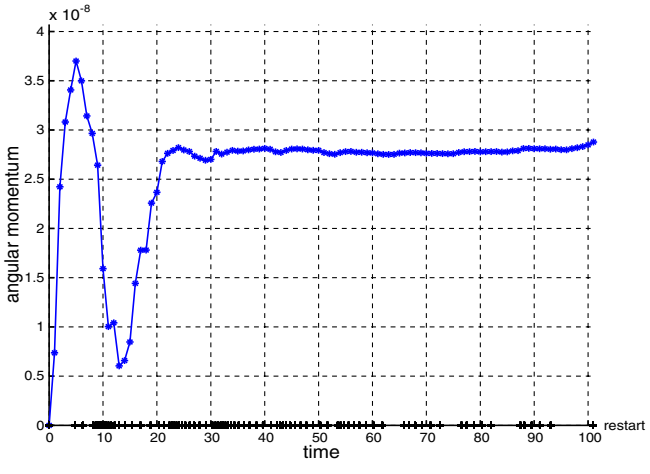

Fig. 16 Total angular momentum of two attracting two-dimensional gas columns (with marked restarts on the time axis)

constant until the columns penetrate. After the collision, an oscillation can be observed.

Figure 16 shows the total angular momentum that is zero in this example. Despite the restarts the change remains in the range of $4 \cdot 10^{-8}$.

6.4 Attracting gas columns rotating in the same direction

For the next numerical example, we consider two rotating gas columns attracting each. For the initial configuration we

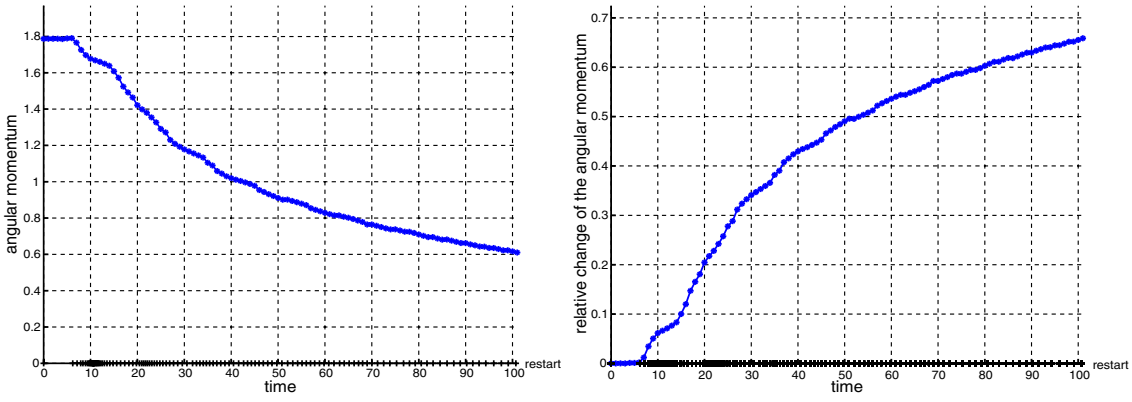

angular momentum relative change of the angular momentum

Fig. 18 Total angular momentum of two attracting gas columns rotating in the same direction and its relative change (with marked restarts on the time axis)

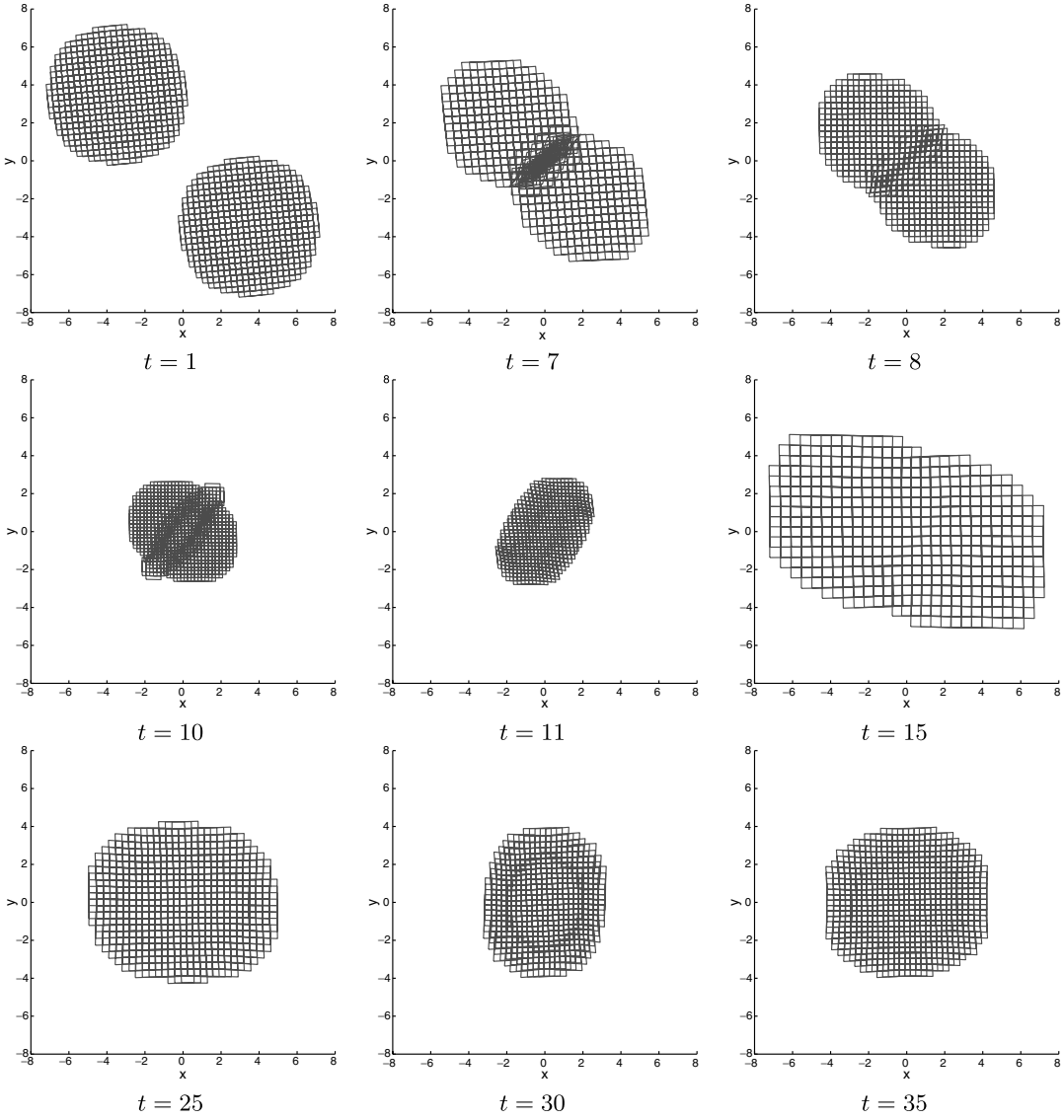

Fig. 19 Particles of two gas columns rotating in the same direction and attracting each other at time t

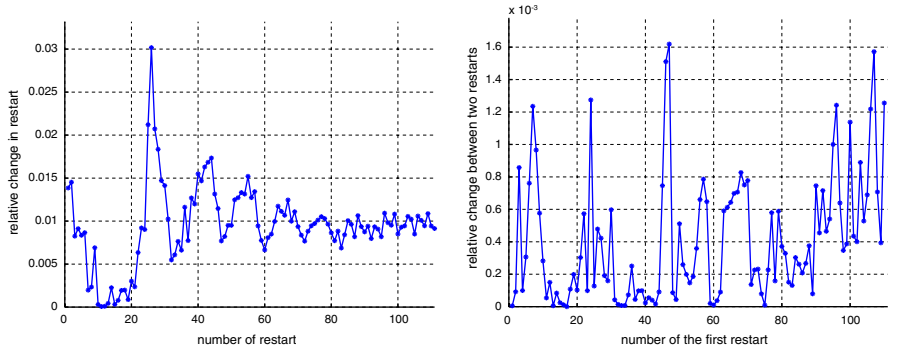

relative change during a restart — relative change between two successive restarts

Fig. 20 Change of the total angular momentum during a and between two successive restarts (asymmetric method)

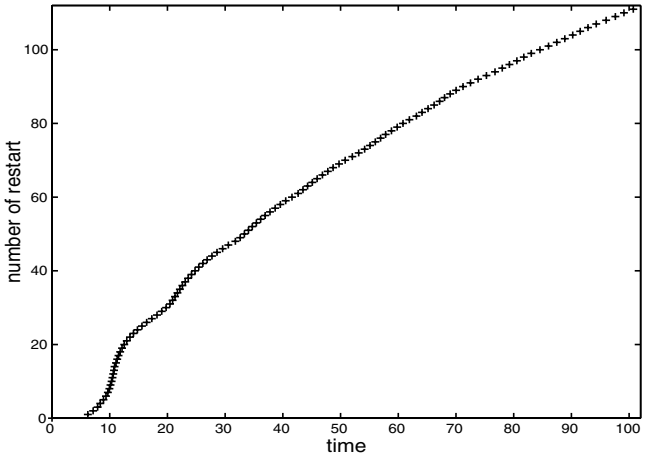

Fig. 17 Restarts of the simulation of two gas columns rotating in the same direction and attracting each other

choose two rotating gas columns in equilibrium. They rotate in the same direction with the same angular velocity $\omega = 0.1$. We start with 650 particles and the simulation is conducted for the time interval [0, 101] with a time step size of $5 \cdot 10^{-3}$. Again, the restarts have to be used. [5] This time, the gas columns are located on the straight line $x = -y$, and thus, the cross sections of the mass density are along this line. At the beginning, the centres of the columns have a non-dimensional distance of about 10.

Unless mentioned otherwise, the asymmetric method is used for the computation of gravitational forces and the refinement criterion is given by the particle size.

In this simulation, 111 restarts occur. In Fig. 17 one can observe that when the gas columns collide (around the time $t = 10$) the frequency of the restarts is highest. This typical behaviour also occurs, if the grid oriented method (110 restarts) or the particle oriented method (109 restarts) are used.

Considering the particles in Fig. 19 one can observe the rotation of the individual columns at the time $t = 1$ and the deformation of the particles when the columns collide ($t = 7, 8, 10$). Again, we can observe the stages of attraction, penetration and the oscillation of the eventual single gas column. Because of the restarts one can hardly see the rotation of the total configuration after the collision. And in fact, in this example the angular momentum is by no means conserved, but the rotation is damped (cf. Fig. 18). The relative change of the total angular momentum is almost 70 percent of the initial angular momentum.

To investigate the deviation of the angular momentum L in more detail, we monitor how it changes during a restart. To this end, we compute

$$\frac{|L(\text{before restart}) - L(\text{after restart})|}{|L(\text{before restart})|}.$$

For comparison, the change of the angular momentum between two successive restarts

$$\frac{|L(t_{\text{restart } i}) - L(t_{\text{restart } i+1})|}{|L(t_{\text{restart } i})|}$$

is considered. In Fig. 20 these data are shown. One can observe that the drift of the total angular momentum is almost entirely due to the restarts. This holds independently of the quadrature policy, see [2].

The energy balance (s. Fig. 21) shows the same behaviour as in the other example of colliding gas columns. We

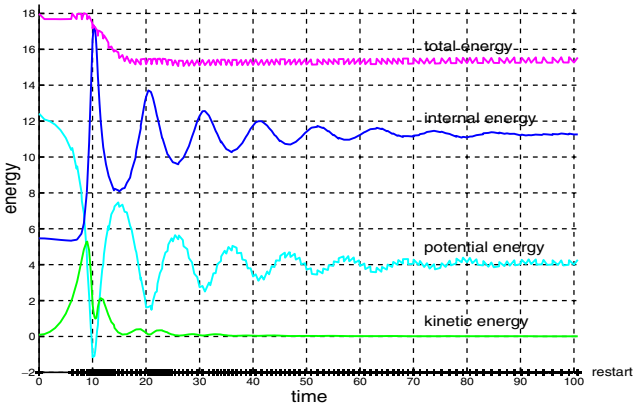

Fig. 21 Energy balance (asymmetric method; ticks mark restarts on the time axis)

[5] For the frictional forces we use $R = 500\rho$ as in the preceding example.

remark that also in the case of the energy the application of particle oriented, grid oriented or asymmetric method does not make much of a difference.

7 Conclusion

We coupled the finite mass method with long range gravitational interactions, where the latter are discretised in an Eulerian framework. The scheme can well cope with massless regions and strongly anisotropic mass distributions, as long as restarts are used to avoid grossly distorted mass packets. The interpolations involved in restarts require a closer examination in order to curb the drift in energy and angular momentum observed in numerical experiments.

Acknowledgements The research of the first and second author was funded by DFG as part of Sonderforschungsbereich 382

References

1. Benz, W.: Smooth particle hydrodynamics – a review. In: Buchler, J.: (ed.), Numerical Modelling of Nonlinear Stellar Pulsations Problems and Prospects, p. 269–. Dordrecht, The Netherlands (1990)
2. Bubeck, T.: The Finite Mass Method with Fields. PhD thesis, Fakultät für Mathematik und Physik, Universität Tübingen, Tübingen, Germany (2003)
3. Chorin, A., Marsden, J.: A Mathmatical Introduction to Fluid Mechanics. Springer, Berlin Heidelberg New York (1993)
4. Courant, R., Friedrichs, K.: Supersonic Flow and Shock Waves. Interscience Publishers, New York (1948)
5. Dautray, R., Lions, J.-L.: Mathematical Analysis and Numerical Methods for Science and Technology, vol. 1. Springer, Berlin (1990)
6. Deuflhard, P., Leinen, P., Yserentant, H.: Concepts of an adaptive hierarchical finite element code. IMPACT Comput. Sci. Eng. **1**, 3–35 (1989)
7. Dubinski, J., Kim, J., Humble, C.P.R.: Gotpm: a parallel hybrid particle-mesh treecode. New Astronomy **9**, 111–126 (2004)
8. Gauger, C.: Erweiterung der Methode der Finiten Massen. PhD thesis, Tübingen, http://w210.ub.uni-tuebingen.de/dbt/volltexte/2000/178/ (2000)
9. Gauger, C., Leinen, P., Yserentant, H.: The finite mass method. SIAM J. Numer. Anal. **37**, 1768–1799 (2000)
10. Griebel, M.: Zur Lösung von Finite-Differenzen- und Finite-Element-Gleichungen mittels der Hierarchischen-Transformations-Mehrgitter-Methode. Technical Report TUM-INFO-01-90-I07-450, SFB 342, Institut für Informatik, TU München, München, Germany (1990)
11. Gurtin, M.: An Introduction to Continuum Mechanics, vol. 158 of Mathematics in Science and Engineering. Academic Press, New York (1981)
12. Hernquist, L., Katz, N.: Treesph – a unification of sph with the hierarchical tree method. Astrophysical Journal, Supplement **70**, 419–446 (1989)
13. Hochbruck, M., Lubich, C.: On Krylov subspace approximations to the matrix exponential operator. SIAM J. Numer. Anal. **34**, 1911–1925 (1997)
14. Klingler, M.: Die Methode der Finiten Massen in der astrophysikalischen Hydrodynamik. PhD thesis, Institut für Physik, Universität Tübingen, Tübingen, Germany (2003)
15. Klingler, M., Leinen, P., Yserentant, H.: The finite mass method on domains with boundary. Report 184, SFB 382, Universität Tübingen, Tübingen, Germany. Submitted to SIAM J. Sci. Comp. (2003)
16. Klingler, M., Leinen, P., Yserentant, H.: A restart procedure for the finite mass method. Report, SFB 382, Universität Tübingen, Tübingen, Germany (2004). In preparation.
17. Landau, L., Lifschitz, E.: Lehrbuch der theoretischen Physik, Mechanik, vol. I. Akademie Verlag, Berlin (1990)
18. Landau, L., Lifschitz, E.: Lehrbuch der theoretischen Physik, Hydrodynamik, volume VI. Akademie Verlag, Berlin (1991)
19. McLean, W.: Strongly Elliptic Systems and Boundary Integral Equations. Cambridge University Press, Cambridge, UK (2000)
20. Monaghan, J.: Smoothed particle hydrodynamics. Annual Review of Astronomy and Astrophysics **30**, 543–574 (1992)
21. Yserentant, H.: A particle model of compressible fluids. Numer. Math. **76**, 111–142 (1997)
22. Yserentant, H.: Entropy generation and shock resolution in the particle model of compressible fluids. Numer. Math. **82**, 161–177 (1999)
23. Yserentant, H.: Particles of variable size. Numer. Math. **82**, 143–159 (1999)
24. Yserentant, H.: The propagation of sound in particle models of compressible fluids. Numer. Math. **88**, 581–601 (2001)
25. Yserentant, H.: The convergence of the finite mass method for flows in given force and velocity fields. In: Griebel, M., Schweitzer, M. (eds.) Meshfree Methods for Partial Differential Equations, vol. 26 of Lecture Notes in Computational Science and Engineering. (2002)